Journal of Magnetism and Magnetic Materials 493 (2020) 165668

Contents lists available at ScienceDirect

Journal of Magnetism and Magnetic Materials

journal homepage: www.elsevier.com/locate/jmmm

Research articles

Structural, electronic and vibrational properties of ultra-thin octahedrally coordinated structure of EuO_2

M. Ozcan[a], S. Ozen[a], M. Yagmurcukardes[b], H. Sahin[a,c,*]

[a] Department of Photonics, Izmir Institute of Technology, 35430 Izmir, Turkey
[b] Department of Physics, University of Antwerp, Groenenborgerlaan 171, B-2020 Antwerp, Belgium
[c] ICTP-ECAR Eurasian Center for Advanced Research, Izmir Institute of Technology, 35430 Izmir, Turkey

ABSTRACT

Novel stable ultra-thin phases of europium oxide are investigated by means of state-of-the-art first principles calculations. Total energy calculations show that single layers of EuO_2 and $Eu(OH)_2$ can be stabilized in an octahedrally coordinated (1T) atomic structure. However, phonon calculations reveal that although both structures are energetically feasible, only the 1T-EuO_2 phase has dynamical stability. The phonon spectrum of 1T-EuO_2 displays three Raman active modes; a non-degenerate out-of-plane A_{1g} mode at 353.5 cm^{-1} and two doubly-degenerate in-plane E_g modes at 304.3 cm^{-1}. Furthermore, magnetic ground state and electronic band dispersion calculations show that the single layer EuO_2 is a metal with net magnetic moment of $5_{\mu B}$ per unitcell resulting in a half-metallic ferrimagnetic behavior. Moreover, robustness of the half-metallic ferrimagnetic characteristics of EuO_2 is confirmed by the application of electric field and charging. Single layer 1T-EuO_2, with its stable ultra-thin structure and half-metallic ferrimagnetic feature, is a promising novel material for nanoscale electronic and spintronic applications.

1. Introduction

Layered materials, that have been studied for more than a century [1], become one of the main focuses of scientific research after the synthesis of graphene by Novoselov et al. [2] Following studies on the layered materials have revealed the existence of novel ultra-thin crystals with extraordinary optical, electrical, mechanical and thermal properties [3–8]. Among ultra-thin materials, transition metal dichalcogenides (TMDs) have gained much attention by scientific community due to their tunable band gap [9,10], low exciton binding energies compared to their bulk form [11–16], field-induced transport with high on-off ratios [17], valley-selective circular dichroism [18–20], and high photovoltaic response properties [21,22]. To overcome the challenges in nanodevice technology, search for novel ultra-thin materials with different functionalities and tunable characteristics is still in progress.

Bulk rare earth compounds have been widely used as high-performance luminescent devices, magnets, catalysts, and functional materials [23]. In addition to their 4*f* electrons originated unique properties in bulk form, Ln-based crystals show more exotic characteristics when their size is reduced down to nanoscale. Tarnuzzer et al. showed that cerium oxide nanoparticles are promising materials for tumor treatment applications in which ceria protects biological systems instead of tumor cells from radiation damage [24]. Geng et al. reported that the anion-exchanged rare-earth hydroxides display RE^{3+} emission making them suitable for optoelectronic device applications [25]. In another study Lee et al. demonstrated the potential of uniform nanocrystalline cerium oxide on practical detection in environmental toxicology for biological applications [26]. Furthermore, Poudret et al. reported the hydrothermally synthesized new lanthanide hydroxyhalides [27].

Among the lanthanide elements, Eu(III) has been the most widely studied one owing to its multiphoton up-conversion properties. There are widespread potential applications for Eu(III), ranging from color displays to biomedical sensors [28–32]. Hudry et al. reported the first nonaqueous approaches used for the synthesis of ultrasmall europium oxide nanoplatelets which are deeply affected by hidden parameters [33]. Also it was claimed that the formation of such wontless polycrystalline form of europium oxide causes an influential impact on the resulting crystal field which is directly related to the photoluminescence properties. Furthermore, Hu et al. reported a successful synthesis method for well-defined Eu hydroxide nanosheets which are promising materials thanks to their unilamellar morphology and photoluminescence (PL) properties for optical devices [34].

Although nanoscale structures of Eu have been widely studied by many groups, there is a lack of literature on its 2D ultra-thin forms. Motivated by recent advances in synthesis techniques and experimental results demonstrating the possibility of octahedral bonding of Eu atoms inside the $Y(OH)_3$ crystals [43], in this study we investigate the structural, phononic, electronic, and magnetic properties of pristine single layer 1T phase of EuO_2 and $Eu(OH)_2$ by using density functional theory (DFT) based calculations.

* Corresponding author.
E-mail address: hasansahin.edu@gmail.com (H. Sahin).

https://doi.org/10.1016/j.jmmm.2019.165668
Received 13 February 2019; Received in revised form 26 July 2019; Accepted 26 July 2019
Available online 03 August 2019
0304-8853/

The paper is organized as follows. Our computational approach is given in Section 2. Ground state structural and vibrational properties of single layer EuO_2 and fully hydrogenated single layer EuO_2 are discussed in Section 3 together with the electronic, magnetic properties and effect of charging and electric field of single layer EuO_2. Section 4 is devoted to conclusions of our results.

2. Computational methodology

To investigate the structural, vibrational, electronic and magnetic properties of single layer EuO_2 and $Eu(OH)_2$, theoretical calculations were carried out in the framework of DFT by using Vienna *ab initio* Simulation Package (VASP) [35,36]. The calculations were performed by using the projector augmented wave (PAW) potentials as implemented in VASP [37,38].

Generalized gradient approximation of the Perdew-Burke-Ernzerhof (GGA-PBE) functional was used for the exchange-correlation energy [39]. The charge transfer between individual atoms was analyzed by the Bader technique [40]. The DFT + U method described by Dudarev was used in order to take into account strong correlations between *d*-orbitals of Eu atoms [41]. In this method, the effective U parameter, which is defined as the difference between the on-site Coulomb parameter and the exchange parameter, $U_{eff} = U - J$, was taken to be 6 eV.

For plane-wave basis set, kinetic energy cutoff was taken to be 500 eV for all the calculations. The total energy difference between the sequential steps as a convergence criterion for ionic relaxations was set to 10^{-5} eV. In the unit cell, the total force was reduced to value less than 10^{-4} eV/Å. Spin-polarized calculations were performed in all cases and Gaussian smearing of 0.01 eV was used for the electronic density of states calculations.

The cohesive energy per atom E_{Coh} was calculated using the formula

$$E_{Coh} = \left[\sum_i n_{atom(i)} E_{atom(i)} - E_{system}\right] / n_{total} \quad (1)$$

where $E_{atom(i)}$ is isolated single atom energy of the i^{th} atom, while i stands for the number of all atoms for the same species, n_{total} represents the total number of atoms, and $n_{atom(i)}$ shows the numbers of the same kind of atoms in the primitive unit cell, respectively. Additionally, dynamical stability of single layer EuO_2 and $Eu(OH)_2$ crystals were investigated via phonon band dispersions calculated by using the PHONOPY code [42].

3. Results and discussion

3.1. Structural properties and dynamical stability

As demonstrated by the recent studies [43], Eu doping in hydroxides such as $Y(OH)_3$ leads to formation of octahedrally bonded europium oxides. Such stable octahedral coordination resembles the 1T phase of TMDs. Therefore, we first examine the stability of possible EuO_2 and $Eu(OH)_2$ crystal structures via total energy and phonon calculations.

Total energy calculations show that both single layers of EuO_2 and $Eu(OH)_2$ structures can be optimized in 1T phase that belongs to $P\bar{3}m1$ space group with the hexagonal Bravais lattice (see Fig. 1(a) and (b)). In EuO_2 structure each Eu atom binds to six O atoms with a bond length of 2.34 Å and the optimized lattice parameters are $a = b = 3.68$ Å. On the other hand, in $Eu(OH)_2$ structure Eu-O bond length is 2.60 Å, while the O–H bond length is found to be 0.97 Å and the optimized lattice constants are $a = b = 3.75$ Å. Bader charge analysis shows that each O atom receives 1.0 *e*/atom from Eu atom in EuO_2 while in $Eu(OH)_2$ H and Eu atoms donate 0.5 and 1.7 *e* to each O atom.

The stability of 1T-EuO_2 and 1T-$Eu(OH)_2$ with respect to other europium phases can be deduced from the cohesive energy per atom. As shown in Fig. 1(c), both structures have cohesive energy indicating their stability and their energy are comparable to other most stable europium oxides.

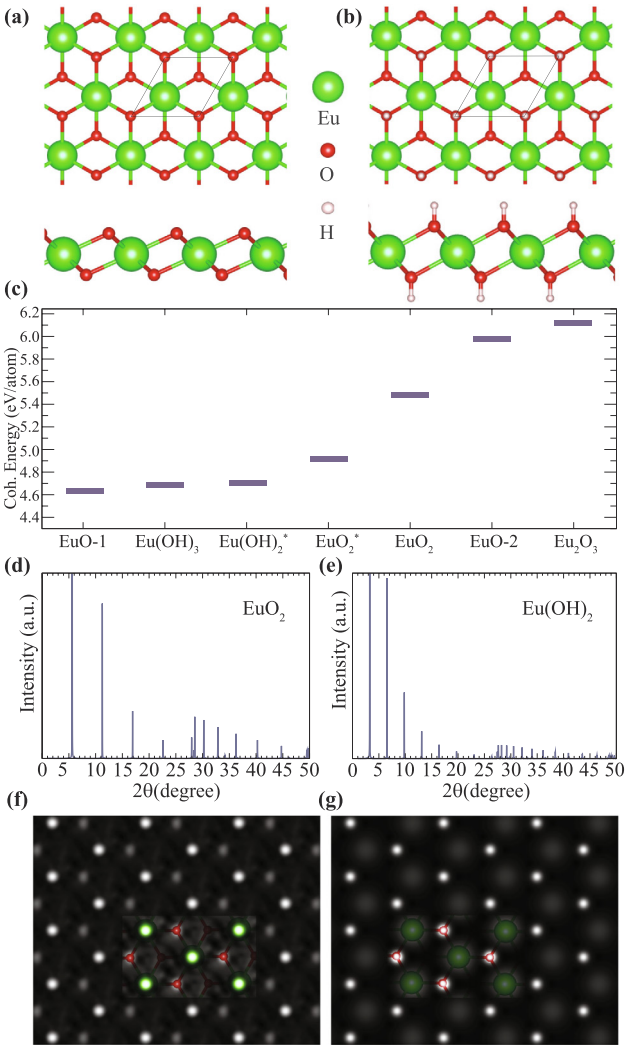

Fig. 1. Top view, side view of (a) EuO_2, (b) $Eu(OH)_2$ from top to bottom, respectively. (c) Cohesive energies per atom of single layer EuO_2, single layer $Eu(OH)_2$, $Eu(OH)_2$, EuO-1(Pm-3 m), EuO-2(Fm-3 m), Eu_2O_3(P-3m1), and EuO_2(P4/nmm). (* stands for single layers) Calculated (d)-(e) X-ray diffractograms and (f)-(g) STM images.

In addition, calculated X-ray diffractograms of single layers EuO_2 and $Eu(OH)_2$ are presented at the bottom panel of Fig. 1(d) and (e), respectively. For the single layer EuO_2, there are four intense signals at 5.5°, 11.0°, 17.0°, and 22.5° 2θ degrees. However, in the presence of H atoms, three additional signals having lower intensities appear at 19.0°, 23.0°, 16.0° and the main signals originated from 1T-EuO_2 are shifted to the lower 2θ degrees (4.0°, 10.0°, 13.0°, 16.0°) with higher intensities. When we compare the peaks of two single layers that appear at 2θ degrees above 25.0°, it is obvious that although the XRD signals of single layer 1T-EuO_2 are more intense, the number of the signals are less in number. Therefore, the H atoms lead to additional signals, the red shift, and the increase in the intensity for the main signals that are obtained at 2θ degrees below 25.0°.

Furthermore, the scanning tunneling microscopy (STM) simulations of EuO_2 and $Eu(OH)_2$ are performed in order to obtain the surface images at the atomic level and presented in Fig. 1(f) and (g), respectively. As seen in Fig. 1(f), Eu atoms appear as bright spots in 1T-EuO_2 crystal. However, neighboring O atoms which are at top of the EuO_2

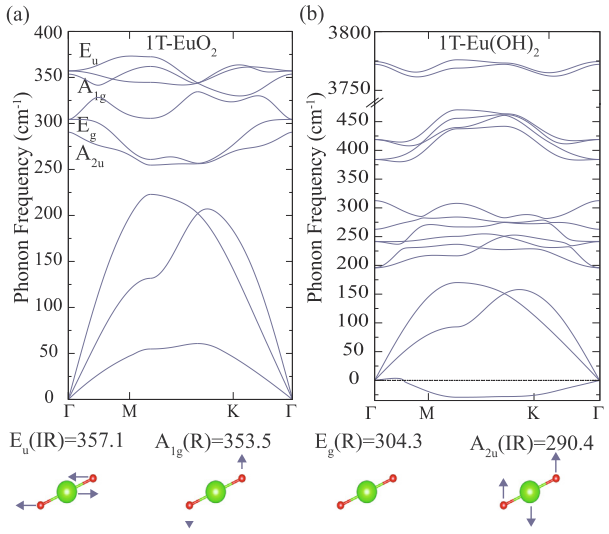

Fig. 2. Phonon band dispersions of (a) EuO_2, (b) $Eu(OH)_2$. The eigenfrequencies for Raman and Infrared-active modes, and the corresponding vibrational motion of the individual atoms are shown at the bottom panel for EuO_2 structure.

surface come into sight as shady white spots. In the case of 1T-$Eu(OH)_2$, since the surface H atoms bind to top of oxygen atoms, the distance between the tip and the europium atoms increases. Therefore, H atoms appear as brighter spots than Eu atoms. The shady white and bright spots form a hexagonal shape consistent with the structures for both EuO_2 and $Eu(OH)_2$.

The energy optimization calculations predicting the total energy, cohesive energy or formation energy of a given structure at 0 K are insufficient for determination of their dynamical stability. Therefore, we examine dynamical stabilities of both single layers via phonon band dispersions through the whole BZ. Vibrational spectrum of single layer 1T-EuO_2 (see Fig. 2(a)) is composed of nine phonon branches at the Γ-point; three acoustic and six optical. The decomposition of the vibration representation of optical modes at the Γ point is $\Gamma_{opt.} = 2E_u + A_{2u} + 2E_g + A_{1g}$. Additionally, LA and TA acoustic branches have an almost linear dispersion. Near the Γ point the out-of-plane flexural (ZA) vibration mode is found to exhibit negative frequencies due to insufficient FFT-grid. Therefore, by fitting the out-of-plane flexural (ZA) mode near the Γ point the imaginary frequencies are corrected. As given at the bottom panel of Fig. 2, there are three Raman active modes one of which is non-degenerate out-of-plane mode while the other two are doubly-degenerate in-plane vibrational modes. As a result, 1T phase of single layer EuO_2 is a dynamicaly stable crystal with its strong Eu-O bonds leading to high frequency phonon modes as single layer $MoSe_2$[44–46].

In addition, as seen in Fig. 2(b), in the case of 1T-$Eu(OH)_2$ two optical phonons having frequency of 3777.3 cm^{-1} are originated from the H-O bond stretching. Analysis of lattice dynamics shows that single layer 1T-$Eu(OH)_2$ has the out-of-plane flexural (ZA) vibration mode lying at the negative frequency regime in the BZ. The restoring forces are nonexistent for ZA optical mode due to the full hydrogenation of EuO_2 which leads to weakening of the Eu-O bonds and charge imbalance on Eu and O atoms. It appears that while the 1T phase of $Eu(OH)_2$ corresponds to a stable structure in terms of total energy optimization calculations.

Therefore, the rest of the paper is devoted to investigation of electronic and magnetic properties of single layer 1T-EuO_2.

3.2. Electronic and magnetic properties

Ground state crystal structure of 1T-EuO_2 is formed by hybridization of two unpaired Eu-4*f* orbital electrons with the two half-filled O-*p* orbitals and resulting charge distribution leads to 7 (1) unpaired electron on Eu (O) atoms. Magnetic charge density ($\rho_{mag} = \rho_{\Uparrow} - \rho_{\Downarrow}$) shown in Fig. 3, reveals that in single layer 1T-EuO_2 crystal Eu atoms with $7_{\mu B}$ and O atoms with $1_{\mu B}$ are antiferromagnetically coupled and opposing magnetic moments unequal at the sublattices result in a $5_{\mu B}$ net magnetic moment per unitcell. Apparently, single layer 1T-EuO_2 crystal is a ferrimagnetic material.

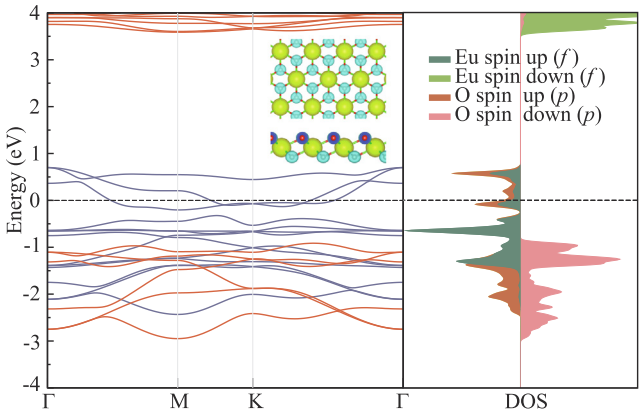

Fig. 3. Electronic band structure and atom-spin decomposed electronic density of states of EuO_2 (inset; Top and side views of spin up-down charge density of EuO_2. The blue lobes correspond to the minority while the yellow lobes correspond to the majority spin density).

Additionally, as shown in Fig. 3, the electronic band dispersion and electronic density of states reveal that single layer 1T-EuO_2 structure shows half-metallic behavior. While it is a semiconductor with 4.5 eV band gap for minority spin components, metallic behavior originates from majority spin states crossing the Fermi level. Two crossing bands at the vicinity of the Fermi level result in three Dirac-cone like dispersions in between M-K, K-Γ and at the K high symmetry point. As seen from the partial density of states presented in Fig. 3, majority spin states around the Fermi level stem from Eu-*f* and O-*p* orbitals.

Up to here, freestanding form of single layer 1T-EuO_2 crystal is considered. However, surface induced effects such as strain and charging may lead to slight distortion in the atomic arrangement which directly determines the electronic structure of the material. Therefore, examination of the robustness of the half-metallic ferrimagnetic behavior is of importance.

In order to investigate the effect of external field on the electronic properties of 1T-EuO_2, we consider an out-of-plane electric field varying between ±0.3 eV/Å. Firstly, it is seen from the charge density analysis that the applied electric field slightly breaks the charge symmetry on the uppermost and lowermost O atoms. As shown in Fig. 4, such charge imbalance in the out-of-plane direction leads to significant splittings in electronic bands formed by O-p_z states. Apparently, despite the E-field induced splittings around the Fermi level, 1T-EuO_2 maintains its halfmetallic ferrimagnetic behavior.

As an external effect, charging is an effective strategy to tune the electronic properties of a material and it can be applied by a substrate or an electronic gate. In order to investigate the effect of charging on its electronic band dispersion, ±0.05 and ±0.10 *e* charging per unitcell applied to the single layer 1T-EuO_2. It is seen that while added/removed charges mostly affects the charge distribution on O atoms, charging has a negligible effect on Eu atoms. Structurally, only the thickness of the single layer structure is modified by charging. Here it is found that the higher the amount of charging the larger the thickness. As shown the right panel of Fig. 4, while charging has no effect on the dispersion of electronic states in BZ, it directly determines the Fermi level by band filling or emptying. It worths to be noted that due to the robust electronic band structure of the single layer 1T-EuO_2 half-

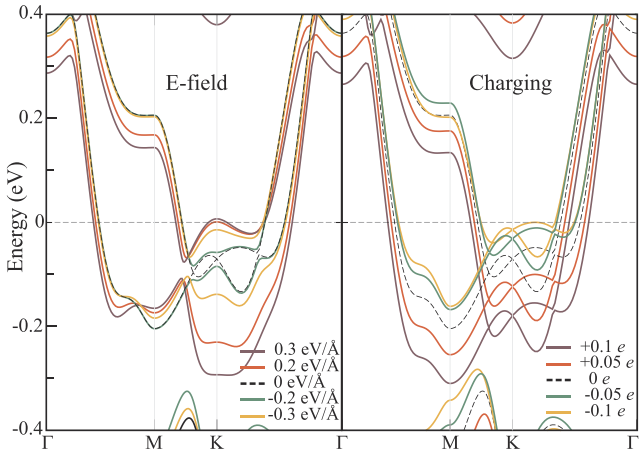

Fig. 4. Electronic band dispersions under electric field (left panel) and charging (right panel).

metallic ferrimagnetic character survives even under higher charging cases.

4. Conclusions

In summary, structural, vibrational and electronic properties of single layer 1T-EuO_2 and 1T-$Eu(OH)_2$ were investigated by means of first principles calculations. While according to total energy calculations both crystal structures are energetically favorable phases, phonon calculations revealed that only the single layer of 1T-EuO_2 is dynamically stable. Additionally, structural fingerprints of both structures were predicted from calculated X-ray diffractograms and STM images. It was also showed that 1T-EuO_2 structure has two prominent peaks (at 304.3 and 353.5 cm^{-1}) in the Raman spectrum.

Electronic band structure calculations revealed that dynamically sTable 1T-EuO_2 structure is a half-metallic ferrimagnet. Robustness of the unique electronic behavior was also examined under external out-of-plane electric field and charging. With its dynamically stable, ultra-thin atomic structure, and robust half-metallic ferrimagnetic electronic nature, 1T-EuO_2 may become an important candidate for spintronics applications.

Acknowledgments

Computational resources were provided by TUBITAK ULAKBIM, High Performance and Grid Computing Center (TR-Grid e-Infrastructure). HS acknowledges financial support from the TUBITAK under the project number 117F095. MY is supported by the Flemish Science Foundation (FWO-Vl) by a postdoctoral fellowship.

Appendix A. Supplementary data

Supplementary data associated with this article can be found, in the online version, athttps://doi.org/10.1016/j.jmmm.2019.165668.

References

[1] B.C. Brodie, On the atomic weight of graphite, Philos. Trans. R. Soc. London 149 (1859) 249.
[2] K.S. Novoselov, A.K. Geim, S.V. Morozov, D. Jiang, Y. Zhang, S.V. Dubonos, I.V. Grigorieva, A.A. Firsov, Electric field effect in atomically thin carbon films, Science 306 (2004) 666.
[3] C. Ataca, H. Sahin, S. Ciraci, Single-layer MX_2 transition-metal oxides and dichalcogenides in a honeycomb-like structure, J. Phys. Chem. C 116 (2012) 8983.
[4] P. Miró, M. Audiffred, T. Heine, An atlas of two-dimensional materials, Chem. Soc. Rev. 43 (2014) 6537.
[5] M. Chhowalla, H.S. Shin, G. Eda, L.J. Li, K.P. Loh, H. Zhang, The chemistry of two-dimensional layered transition metal dichalcogenide nanosheets, Nat. Chem. 5 (2013) 263.
[6] Q.H. Wang, K. Kalantar-Zadeh, A. Kis, J.N. Coleman, M.S. Strano, Electronics and optoelectronics of two-dimensional transition metal dichalcogenides, Nat. Nanotech. 7 (2012) 699.
[7] G.R. Bhimanapati, Z. Lin, V. Meunier, Y. Jung, J. Cha, S. Das, D. Xiao, Y. Son, M.S. Strano, V.R. Cooper, L. Liang, S.G. Louie, E. Ringe, Wu. Zhou, S.S. Kim, R.R. Naik, B.G. Sumpter, H. Terrones, F. Xia, Y. Wang, J. Zhu, D. Akinwande, N. Alem, J.A. Schuller, R.E. Schaak, M. Terrones, J.A. Robinson, Recent advances in two-dimensional materials beyond graphene, ACS Nano 9 (2015) 11509.
[8] D. Akinwande, N. Petrone, J. Hone, Two-dimensional flexible nanoelectronics, Nat. Commun. 5 (2014) 5678.
[9] S.W. Han, H. Kwon, S.K. Kim, S. Ryu, W.S. Yun, D.H. Kim, J.H. Hwang, J.S. Kang, J. Baik, H.J. Shin, S.C. Hong, Band-gap transition induced by interlayer van der Waals interaction in MoS_2, Phys. Rev. B 84 (2011) 045409.
[10] J.K. Ellis, M.J. Lucero, G.E. Scuseria, The indirect to direct band gap transition in multilayered MoS_2 as predicted by screened hybrid density functional theory, Appl. Phys. Lett. 99 (2011) 261908.
[11] D.Y. Qiu, F.H. da Jornada, S.G. Louie, Optical Spectrum of: Many-Body Effects and Diversity of Exciton States, Phys. Rev. Lett. 111 (2013) 216805.
[12] A. Chernikov, T.C. Berkelbach, H.M. Hill, A. Rigosi, Y. Li, O.B. Aslan, D.R. Reichman, M.S. Hybertsen, T.F. Heinz, Exciton Binding Energy and Nonhydrogenic Rydberg Series in Monolayer WS_2, Phys. Rev. Lett. 113 (2014) 076802.
[13] K. He, N. Kumar, L. Zhao, Z. Wang, K.F. Mak, H. Zhao, J. Shan, Tightly bound excitons in monolayer WSe_2, Phys. Rev. Lett. 113 (2014) 026803.
[14] A. Ramasubramaniam, Large excitonic effects in monolayers of molybdenum and tungsten dichalcogenides, Phys. Rev. B 86 (2012) 115409.
[15] Z. Ye, T. Cao, K. O'Brien, H. Zhu, X. Yin, Y. Wang, S.G. Louie, X. Zhang, Probing excitonic dark states in single-layer tungsten disulphide, Nature 513 (2014) 214.
[16] M.M. Ugeda, A.J. Bradley, S.-F. Shi, F.H. da Jornada, Y. Zhang, D.Y. Qiu, W. Ruan, S.-K. Mo, Z. Hussain, Z.-X. Shen, S.G. Louie, M.F. Crommie, Giant bandgap renormalization and excitonic effects in a monolayer transition metal dichalcogenide semiconductor, Nat. Mater. 13 (2014) 1091.
[17] B. Radisavljevic, A. Radenovic, J. Brivio, V. Giacometti, A. Kis, Single-layer MoS_2 transistors, Nat. Nanotech. 6 (2011) 147.
[18] K.F. Mak, K.L. He, J. Shan, T.F. Heinz, Control of valley polarization in monolayer MoS_2 by optical helicity, Nat. Nanotech. 7 (2012) 494.
[19] T. Cao, G. Wang, W. Han, H. Ye, C. Zhu, J. Shi, Q. Niu, P. Tan, E. Wang, B. Liu, J. Feng, Valley-selective circular dichroism of monolayer molybdenum disulphide, Nat. Commun. 3 (2012) 1882.
[20] A.M. Jones, H. Yu, N.J. Ghimire, S. Wu, G. Aivazian, J.S. Ross, B. Zhao, J. Yan, D.G. Mandrus, D. Xiao, W. Yao, X. Xu, Optical generation of excitonic valley coherence in monolayer WSe_2, Nat. Nanotech. 8 (2013) 634.
[21] M. Bernardi, M. Palummo, J.C. Grossman, Extraordinary sunlight absorption and one nanometer thick photovoltaics using two-dimensional monolayer materials, Nano Lett. 13 (2013) 3664.
[22] H.R. Gutierrez, N. Perea-López, A.L. Elías, A. Berkdemir, B. Wang, R. Lv, F. López-Urías, V.H. Crespi, H. Terrones, M. Terrones, Extraordinary Room-Temperature Photoluminescence in Triangular WS_2 Monolayers, Nano Lett. 13 (2013) 3447.
[23] M.K. Devaraju, S. Yin, T. Sato, Eu^{3+}:Y_2O_3 Microspheres and microcubes: a supercritical synthesis and characterization, Inorg. Chem. 50 (2011) 4698.
[24] R.W. Tarnuzzer, J. Colon, S. Patil, S. Seal, Vacancy engineered ceria nanostructures for protection from radiation-induced cellular damage, Nano Lett. 5 (2005) 2573.
[25] F. Geng, H. Xin, Y. Matsushita, R. Ma, M. Tanaka, F. Izumi, N. Iyi, T. Sasaki, New layered rare earth hydroxides with anion exchange properties, Chem. Eur. J. 14 (2008) 9255.
[26] S.S. Lee, H. Zhu, E.Q. Contreras, A. Prakash, H.L. Puppala, V.L. Colvin, High temperature decomposition of cerium precursors to form ceria nanocrystal libraries for biological applications, Chem. Mater. 24 (2012) 424.
[27] L. Poudret, T.J. Prior, L.J. McIntyre, A.M. Fogg, Synthesis and crystal structures of new lanthanide hydroxyhalide anion exchange materials, $Ln_2(OH)_5X\ 1.5H_2O$ (X = Cl, Br; Ln = Y, Dy, Er, Yb), Chem. Mater. 20 (2008) 7447.
[28] J. Feng, H. Zhang, Hybrid materials based on lanthanide organic complexes: a review, Chem. Soc. Rev. 42 (2013) 387.
[29] S. Aime, M. Botta, M. Fasano, E. Terreno, Lanthanide (III) chelates for NMR biomedical applications, Chem. Soc. Rev. 27 (1998) 19.
[30] J.D. Moore, R.L. Lord, G.A. Cisneros, M.J. Allen, Concentration-independent pH detection with a luminescent dimetallic Eu (III)-based probe, J. Am. Chem. Soc. 134 (2012) 17372.
[31] M. Zheng, H. Tan, Z. Xie, L. Zhang, X. Jing, Z. Sun, Fast response and high sensitivity europium metal organic framework fluorescent probe with chelating terpyridine sites for Fe^{3+}, ACS Appl. Mater. Interf. 5 (2013) 1078.
[32] S.B.-D. Makhluf, R. Arnon, C.R. Patra, D. Mukhopadhyay, A. Gedanken, P. Mukherjee, H. Breitbart, Labeling of sperm cells via the spontaneous penetration of Eu^{3+} ions as nanoparticles complexed with PVA or PVP, J. Phys. Chem. C 112 (2008) 12801.
[33] D. Hudry, A.M.M. Abeykoon, J. Hoy, M.Y. Sfeir, E.A. Stach, J.H. Dickerson, Ultrathin europium oxide nanoplatelets: hidden parameters and controlled synthesis, unusual crystal structure, and photoluminescence properties, Chem. Mater. 27 (2015) 965.
[34] L. Hu, R. Ma, T.C. Ozawa, T. Sasaki, Exfoliation of layered europium hydroxide into unilamellar nanosheets, Chem. Asian J. 5 (2010) 248.
[35] G. Kresse, J. Hafner, Ab initio molecular dynamics for liquid metals, Phys. Rev. B 47 (1993) 558.
[36] G. Kresse, J. Furthmüller, Efficient iterative schemes for ab initio total-energy calculations using a plane-wave basis set, Phys. Rev. B 54 (1996) 11169.

[37] G. Kresse, D. Joubert, From ultrasoft pseudopotentials to the projector augmented-wave method, Phys. Rev. B 59 (1999) 1758.
[38] P.E. Blöchl, Projector augmented-wave method, Phys. Rev. B 50 (1994) 17953.
[39] J.P. Perdew, K. Burke, M. Ernzerhof, Generalized gradient approximation made simple, Phys. Rev. Lett. 77 (1996) 3865.
[40] G. Henkelman, A. Arnaldsson, H. Jónsson, A fast and robust algorithm for Bader decomposition of charge density, Comp. Mater. Sci. 36 (2006) 354.
[41] S.L. Dudarev, G.A. Botton, S.Y. Savrasov, C.J. Humphreys, A.P. Sutton, Electron-energy-loss spectra and the structural stability of nickel oxide: An LSDA+ U study, Phys. Rev. B 57 (1998) 1505.
[42] A. Togo, F. Oba, I. Tanaka, First-principles calculations of the ferroelastic transition between rutile-type and $CaCl_2$-type SiO_2 at high pressures, Phys. Rev. B 78 (2008) 134106.
[43] T. Guner, A. Kus, M. Ozcan, A. Genc, H. Sahin, and M.M. Demir, Green Fabrication of $Y(OH)_3$: Eu3+ Nanoparticles for White Light Generation, arXiv:1811.09478.
[44] S. Horzum, H. Sahin, S. Cahangirov, P. Cudazzo, A. Rubio, T. Serin, F.M. Peeters, Phonon softening and direct to indirect band gap crossover in strained single-layer $MoSe_2$, Phys. Rev. B 87 (2013) 125415.
[45] A. Splendiani, L. Sun, Y. Zhang, T. Li, J. Kim, C.Y. Chim, G. Galli, F. Wang, Emerging photoluminescence in monolayer MoS_2, Nano Lett. 10 (2010) 1271.
[46] X. Wang, Y. Gong, G. Shi, W.L. Chow, K. Keyshar, G. Ye, R. Vajtai, J. Lou, Z. Liu, E. Ringe, B.K. Tay, P.M. Ajayan, Chemical vapor deposition growth of crystalline monolayer $MoSe_2$, ACS Nano 8 (2014) 5125.